ELSEVIER

Polymer 42 (2001) 9617–9626

polymer

www.elsevier.com/locate/polymer

Crystalline memory effect in isothermal crystallization of syndiotactic polypropylenes: effect of fusion temperature on crystallization and melting behavior

Pitt Supaphol[a,*], Jar-Shyong Lin[b]

[a]*The Petroleum and Petrochemical College, Chulalongkorn University, Soi Chulalongkorn 12 Phyathai Road, Pathumwan, Bangkok 10330, Thailand*
[b]*Solid State Division, Oak Ridge National Laboratory, Oak Ridge, TN 37831, USA*

Received 14 February 2001; received in revised form 22 May 2001; accepted 12 June 2001

Abstract

In this manuscript, studies on the crystalline memory effect in syndiotactic polypropylene (s-PP) were focused on the effect of prior melt annealing on the subsequent isothermal crystallization kinetics, crystalline structure, lamellar morphology, and subsequent melting behavior using a combination of differential scanning calorimetry (DSC), wide-angle X-ray diffraction (WAXD), and small-angle X-ray scattering (SAXS) techniques. On partial melting, choices of the fusion temperature used to melt the samples played an important role in determining the overall rate of isothermal crystallization, while they had no effect on the resulting values of the apparent crystallinity content, the long period, the lamellar thickness, and the low-melting peak temperature.

Keywords: Crystalline memory effect; Partial melting; Complete melting

1. Introduction

It is well established that nucleation mechanisms play an important role in crystallization of polymers either from solution or from melt. Nucleation mechanisms can be categorized into two main processes: primary and secondary nucleation (i.e. subsequent crystal growth). Primary nucleation is defined as the origination of crystalline phase from the polymer solution or the melt. It can be categorized into two types depending on the physical origins of the nucleus (i.e. chemical make-up of the critical nucleus when comparing with that of the surface onto which the critical nucleus is formed): homogeneous and heterogeneous nucleation. Secondary nucleation is defined as a surface nucleation on an existing growth face, which is responsible for further growth of the activated nucleus.

In actual processings of a semicrystalline polymer, primary nucleation mechanism and rate are characterized and controlled mainly by not only the presence of infusible heterogeneous nuclei (e.g. catalyst residues, nucleation agents, impurities, etc.), but the processing history (viz. dictated by temperature, pressure, stress, etc.) as well. Because of their importance in determining overall crystallization kinetics and morphology, it is necessary that the nucleation mechanism and rate are better understood. It is therefore very important that the influences of impurities, additives, nucleating agents, and especially 'crystalline memory effect' on crystallization behavior be thoroughly investigated. The latter refers to clusters of molecules that retain their crystallographic arrangement of crystals as a result of insufficient or partial melting conditions, and, upon subsequent cooling, these aggregates of clusters of molecules can act as predetermined athermal nucleation sites (provided they exceed the critical nucleus size, required for crystallization at a specific temperature) which can greatly enhance the overall crystallization rate. This phenomenon is also referred to as 'self-nucleation effect.'

Since, in actual polymer processings, a polymer part is not only subjected to thermal treatments, but to mechanical manipulations as well. Such mechanical deformational histories can lead to preferred orientation of polymer molecules which in itself can enhance nucleation rate. This effect is referred to as 'orientational memory effect'. Both types of memory effects can greatly affect the crystallization behavior during subsequent cooling of the polymer part. To eliminate both kinds of memory effects, it is necessary to keep the part at a sufficiently high fusion temperature T_f for a sufficiently long period of time (depending on the

* Corresponding author. Tel.: +66-2-218-4134; fax: +66-2-215-4459.
E-mail address: pitt.s@chula.ac.th (P. Supaphol).

0032-3861/01/$ - see front matter
PII: S0032-3861(01)00507-9

fusion temperature T_f used) in order to eradicate as many traces of crystalline and oriented aggregates as possible (i.e. complete melting). Practically, a fusion temperature T_f for attaining complete melting is chosen such that it is greater than the equilibrium melting temperature T_m^0 of the polymer of interest ($T_f > T_m^0$). In some cases however, we wish to use these memory effects to preferably control the overall crystallization rate or morphology of the crystallizing polymer. Thus, we need to understand the characteristics of these effects in detail.

Due to their important influence on the crystallization behavior of polymers, memory effects (i.e. either in the context of the crystalline or orientation memory effect, or both) have been of considerable interest and have been studied by several investigators [1–15]. Recently, Supaphol and Spruiell [16] have reported studies on the crystalline memory effects in isothermal crystallization of syndiotactic polypropylene (s-PP), which were mainly dealt with the effects of heating rate ϕ, fusion temperature T_f, and holding time t_h on the effective total concentration of predetermined nuclei N_{tot} and the effective average spherulite diameter D.

In this manuscript, we focus on the effect of prior melt annealing on the subsequent isothermal crystallization kinetics, crystalline structure, lamellar morphology, and subsequent melting behavior of three commercial grade s-PP resins using a combination of differential scanning calorimetry (DSC), wide-angle X-ray diffraction (WAXD), and small-angle X-ray scattering (SAXS) techniques. This can be carried out by studying subsequent isothermal and melting behavior of s-PP samples melted at various choices of the fusion temperature T_f for a fixed holding time t_h. Even though the effect of T_f on the crystallization kinetics of polymers and the interpretation of such an effect based on the concept of self-nucleation have been well-documented (see, for example, Refs. [1–15]), it is guaranteed to the best of our knowedge that there have not been prior studies of s-PP on the similar aspects.

2. Theoretical background

Isothermal bulk crystallization kinetics of semicrystalline polymers is commonly analyzed from the DSC crystallization exotherms [17–19] based primarily on the assumption that the evolution of crystallinity is linearly proportional to the evolution of heat released during the course of crystallization. Based on this notion, the relative crystallinity as a function of time $\theta(t)$ can be obtained according to the following equation:

$$\theta(t) = \frac{\int_0^t \left(\frac{dH_c}{dt}\right) dt}{\int_0^\infty \left(\frac{dH_c}{dt}\right) dt} \in [0,1], \quad (1)$$

where t and $t = \infty$ are the elapsed time during the course of crystallization and at the end of crystallization process, respectively, and dH_c is the enthalpy of crystallization released during an infinitesimal time interval dt.

In order to quantitatively describe the macroscopic evolution of crystallinity during primary crystallization under quiescent isothermal conditions, a number of macrokinetic models have been proposed over the past sixty years: they are, for examples, the so-called 'Avrami' [20–26], the Tobin [27–29], the Malkin [30], and the Urbanovici–Segal [31] models. Very recently, qualitative comparison among the four macrokinetic models was performed on isothermal crystallization data of s-PP [32]. The results suggested that the isothermal crystallization data of s-PP were best described by the Urbanovici–Segal model, followed by the Avrami, Malkin, and Tobin models, respectively. Since the kinetics information obtained from both Avrami and Urbanovici–Segal models is related and is comparatively of great interest, the isothermal crystallization data obtained in this study are analyzed according to these two models.

In the Avrami model [20–26], the relative crystallinity as a function of time $\theta(t)$ relates to the crystallization time t according to the equation:

$$\theta(t) = 1 - \exp[-(K_a t)^{n_a}] \in [0,1], \quad (2)$$

where K_a and n_a are the Avrami crystallization rate constant and the Avrami exponent, respectively. It should be noted that both K_a and n_a are constants specific to a given crystalline morphology and type of nucleation for a particular crystallization condition [33], and the dimension of K_a is given in $[\text{time}]^{-1}$.

While in the Urbanovici–Segal model [31], which is essentially a generalization of the Avrami model, the relationship between the relative crystallinity as a function of time $\theta(t)$ and the crystallization time t is written as

$$\theta(t) = 1 - [1 + (r-1)(K_{us} t)^{n_{us}}]^{1/(1-r)} \in [0,1], \quad (3)$$

where K_{us} and n_{us} are the Urbanovici–Segal crystallization rate constant and the Urbanovici–Segal exponent, respectively. r is a parameter satisfying the condition $r > 0$. At the condition where $r \to 1$, the Urbanovici–Segal model becomes identical to the Avrami model [31]. This simply means that parameter r is merely the factor determining the degree of deviation of the Urbanovici–Segal model from the Avrami model. It is also worth noting that both K_{us} and n_{us} have similar physical meanings to the Avrami kinetics parameters (i.e. K_a and n_a), and that the dimension of K_{us} is also given in $[\text{time}^{-1}]$.

3. Experimental details

3.1. Materials

The s-PP resins used in this study were supplied in pellet form by Fina Oil and Chemical Company (La Porte, Texas, USA). Molecular characterization of these materials was

Table 1
Characterization data of as-received syndiotactic polypropylene resins

Sample	Intrinsic viscosity (dl g^{-1})	M_n	M_w	M_z	M_w/M_n	Racemic pentads (%rrrr)	Racemic triads (%rr)	Racemic dyads (%r)	Ethylene content (Wt%)
s-PP#1	1.61	76 200	165 000	290 000	2.2	77.1	87.3	91.4	1.3
s-PP#2	1.80	52 300	195 000	450 000	3.7	74.6	83.1	87.4	0.6
s-PP#4	1.61	81 300	171 000	294 000	2.1	74.6	84.4	89.2	0.3

carried out by Dr Roger A. Phillips and his coworkers at Basell USA, Inc. (Elkton, Maryland, USA). The results are listed in Table 1. It should be noted that the unusually high degree of polydispersity observed for s-PP#2 resin is due to the bimodal molecular weight distribution the resin exhibits.

3.2. Sample preparation

The standard film for each s-PP resin was prepared from sliced pellets melt-pressed at 190°C between a pair of polyimide films which in turn were sandwiched between a pair of stainless steel platens, in a Wabash compression molding machine under a pressure of 4.62×10^2 MN m^{-2}. After 10 min holding time, the film of ca. 280 μm thick was taken out and allowed to cool at the ambient condition down to room temperature between the two metal platens. This treatment assumes that previous thermo-mechanical history was essentially erased, and provides a standard crystalline memory condition for the as-prepared film.

3.3. Experimental procedures and techniques

In order to gain a complete understanding towards the effect of partial or complete melting on isothermal crystallization and subsequent melting behavior of these s-PP resins, two separate experiments were carried out. The first was to use DSC technique to investigate the effect of partial or complete melting on the behavior of isothermal crystallization as well as the kinetics of the process (hereafter referred to as the DSC experiment), while the second was to use a combination of WAXD, SAXS, and DSC techniques to investigate the effect of partial or complete melting on the morphological aspect of isothermal crystallization and subsequent melting behavior (hereafter referred to as the WAXD/SAXS/DSC experiment).

3.3.1. The DSC Experiment

In this experiment, a DSC (DSC-7, Perkin–Elmer) was used to follow isothermal crystallization and subsequent melting behavior of these s-PP resins. Calibration for the temperature scale was carried out using a pure indium standard ($T_m^0 = 156.6$°C and $\Delta H_f^0 = 28.5\ J\ g^{-1}$) on every other run to ensure accuracy and reliability of the data obtained. To minimize thermal lag between polymer sample and DSC furnace, each sample holder was loaded with a cut piece from the as-prepared films, each of which weighed around 4.8 ± 0.2 mg. It is worth noting that each sample was used only once and all the runs were carried out under nitrogen atmosphere to prevent extensive thermal degradation.

The experiment started with heating each sample from −40°C at a heating rate of 80°C min^{-1} to a desired fusion temperature T_f, ranging from 128 to 200°C. In order to minimize the number of variable parameters, the time interval of the sample was kept at each specified T_f (i.e. the holding time t_h) was fixed for 5 min. After this period, each sample was rapidly cooled (i.e. around 200°C min^{-1}) from T_f to a fixed crystallization temperature T_c of 85°C, where it was held until the crystallization process was considered complete (when no significant change in the heat flow as a function of time was further observed). The isothermal crystallization exotherms and the subsequent melting endotherms recorded at a heating rate of 20°C min^{-1} for various values of T_f were further analyzed to obtain relevant information on the effect of partial or complete melting on isothermal crystallization and subsequent melting behavior of these s-PP resins.

3.3.2. The WAXD/SAXS/DSC experiment

The notion of this experiment was to simulate the conditions set forth in the DSC experiment so that the information related to the morphological aspect can be obtained via the employment of a combination of WAXD, SAXS, and DSC techniques. The 'test' samples used in this experiment (performed only on s-PP#2 resin) were cut from the as-prepared film into a circular shape having a diameter of ca. 1 cm, placed between two clean glass slides, and brought to melt in a Mettler hot-stage at a desired fusion temperature T_f, ranging from 130 to 190°C. After the 5 min holding time at each T_f, the samples were quickly transferred to isothermally crystallize in another Mettler hot-stage at the crystallization temperature T_c of 85°C. After complete crystallization at T_c, the samples were quenched in liquid nitrogen to minimize further change in the morphology and crystallinity. Finally, SAXS and WAXD techniques were employed on these 'test' samples to acquire related information on morphological aspects, while DSC technique was used to obtain related information on subsequent melting behavior (the melting endotherms were recorded at a heating rate of 20°C min^{-1}) of these samples. The same measurements were also carried out on a 'blank' sample, which was cut from the as-prepared film into the dimension and shape similar to those of the 'test' samples. The information obtained on the 'test' samples will

be compared with that obtained on the 'blank' sample so that solid conclusion can be drawn.

The WAXD intensity patterns were collected on a Rigaku–Denki 12 kW rotating anode generator and diffractometer equipped with a computerized data collection and analytical system. The monochromatized X-ray beam was CuK_α radiation ($\lambda = 1.54$ Å). The operating condition of the X-ray source was set at a voltage of 35 kV and a current of 40 mA.

The SAXS intensity data were collected on the ORNL 10-m SAXS instrument [34,35], with a sample-to-detector distance of 5.12 m using CuK_α radiation ($\lambda = 1.54$ Å) and a 20×20 cm^2 two-dimensional position-sensitive area detector with each virtual cell element size of about 3 mm apart. Corrections were made for instrumental backgrounds, dark current due to cosmic radiation and electronic noises in the detector circuitry, and the detector non-uniformity and efficiency (via an Fe^{55} radioactive isotope standard which emits X-rays isotropically by electron capture) on a cell-by-cell basis. The intensity data were azimuthally averaged at each scattering vector q (i.e. $q = (4\pi/\lambda)\sin(\theta/2)$, where λ is the X-ray wavelength and θ the scattering angle) ranging from 0.058 to 1.004 nm^{-1}, and converted to an absolute differential scattering cross section by means of pre-calibrated secondary standards [36]. It should be noted that absolute intensity has a unit of [cm^{-1}].

4. Results and discussion

4.1. Effect of fusion temperature on crystallization behavior

Fig. 1 illustrates, respectively, the time-dependent relative crystallinity function $\theta(t)$ (after subtraction of the induction time t_0) for s-PP#1 samples isothermally crystallized at $T_c = 85$°C after being melted partially at fusion temperatures T_f of 128, 130, and 140°C and after being melted completely at T_f of 180°C for a fixed holding time t_h of 5 min (the raw data are shown as different geometrical points). Qualitatively, the time to reach the ultimate crystallinity (i.e. complete crystallization) increases with increasing fusion temperature T_f used. This clearly suggests that even though the samples were isothermally crystallization at the same temperature, the choice of the fusion temperatures used to melt the samples plays an important role in determining the crystallization behavior. Quantitatively, the half-time of crystallization $t_{0.5}$, which is defined as the elapsed crystallization time from the onset to 50% completion and can be determined directly from the experimental $\theta(t)$ data, can be used to describe the effect of fusion temperature on crystallization behavior. According to Fig. 1, the half-time of crystallization $t_{0.5}$ obtained for s-PP#1 samples partially melted at $T_f = 128$, 130, and 140°C is 1.0, 1.7, and 3.5 min, respectively, while that for sample completely melted at $T_f = 180$°C is 5.6 min.

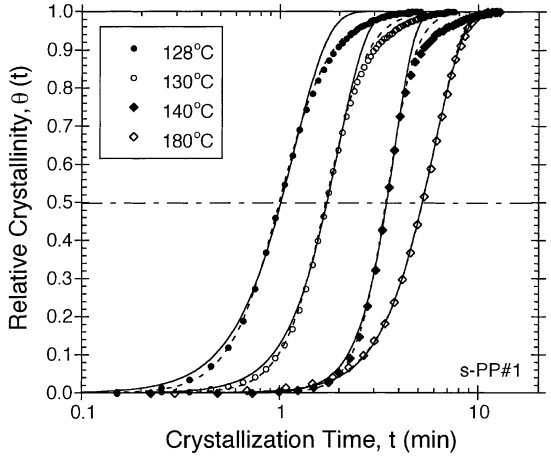

Fig. 1. Variation of the relative crystallinity $\theta(t)$ as a function of crystallization time t for s-PP#1 samples isothermally crystallized at 85°C after being melted at each respective fusion temperature T_f for 5 min. The raw data, shown as various geometrical points, were fitted to the Avrami and Urbanovici–Segal macrokinetic models, in which the best fits are shown as solid and dashed lines, respectively.

Fig. 2 illustrates plots of crystallization half-time $t_{0.5}$ as a function of the fusion temperature T_f, ranging from 128 to 200°C, for all of s-PP resins studied. Apparently, the observed $t_{0.5}$ values and the overall rate of crystallization (presented in Fig. 3 in the form of reciprocal values of the crystallization half-time, i.e. $t_{0.5}^{-1}$) exhibit strong correlations with the fusion temperature within the range $T_f \leq$ ca. 160°C, while they become independent of the fusion temperature within the range $T_f \geq$ ca. 160°C. For all of the resins studies, within the range $T_f \leq$ ca. 160°C, values of the crystallization half-time were found to increase monotonically, while those of the reciprocal half-time decrease, with increasing fusion temperature. After the critical T_f value of 160°C however, both the crystallization half-time and its reciprocal value become independent of the fusion temperature used. The results clearly suggested that prolonged melting of these s-PP resins at $T_f \geq$ ca. 160°C for the fixed holding time t_h

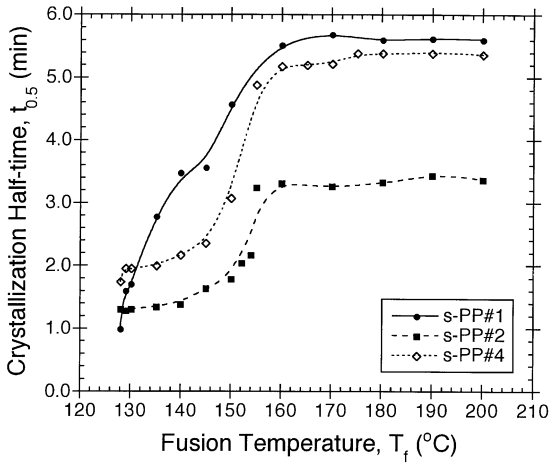

Fig. 2. Variation of the crystallization half-time $t_{0.5}$ as a function of the fusion temperature T_f used to melt the samples for all of the s-PP resins studied.

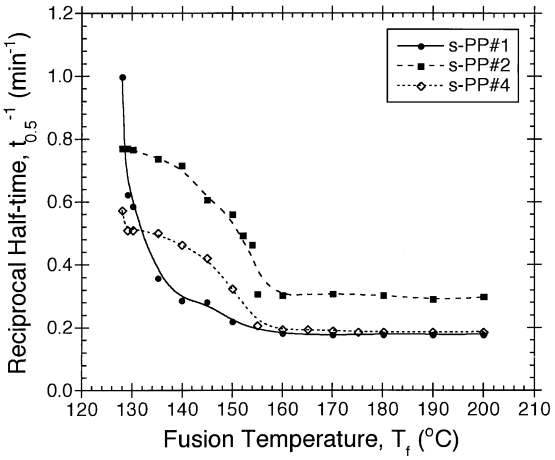

Fig. 3. Variation of the reciprocal value of the crystallization half-time (i.e. $t_{0.5}^{-1}$) as a function of the fusion temperature T_f used to melt the samples for all of the s-PP resins studied.

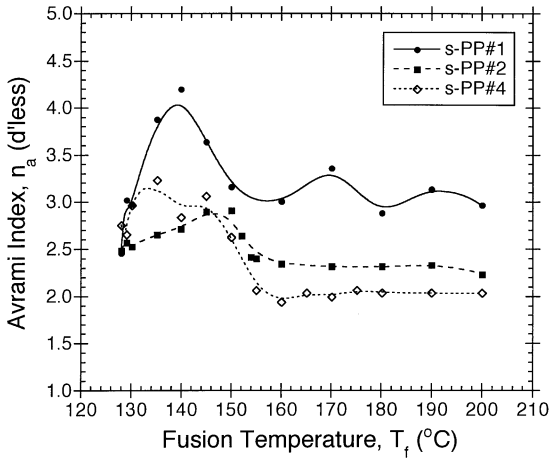

Fig. 4. Variation of the Avrami index n_a as a function of the fusion temperature T_f used to melt the samples for all of the s-PP resins studied.

of 5 min is mandatory in order for any measurement on crystallization behavior to be free from the influences of the self-nucleation effect.

Comparatively, s-PP#1 resin crystallizes faster than s-PP#2 and s-PP#4 resins within the range $T_f \leq$ ca. 129°C and where $T_f \leq$ ca. 133°C, respectively. Beyond these ranges, s-PP#1 resin crystallizes the slowest, followed by s-PP#4 and s-PP#2 resins, respectively. This finding agrees extremely well with earlier reports on isothermal and non-isothermal bulk crystallization studies of these resins [37,38] that the crystallization ability of these resins follows the following order: s-PP#2 > s-PP#4 > s-PP#1. Interestingly, despite the much difference in the molecular weight characteristics among these resins, the critical fusion temperatures T_f required for achieving the complete melting conditions of these resins are technically identical (i.e. ca. 160°C).

4.2. Effect of fusion temperature on crystallization kinetics

In order to observe the effect of partial and complete melting conditions on the kinetics of crystallization, the experimental $\theta(t)$ data collected on all resins were analyzed according to the Avrami and the Urbanovici–Segal models (i.e. Eqs. (2) and (3), respectively) using the direct data-fitting procedure [39]. The two models were chosen mainly because it was shown in a recent report [32] that isothermal crystallization data of s-PP#4 resin was best described by the two models (with the Urbanovici–Segal model being the better of the two).

4.2.1. Avrami analysis

Data analysis based on the Avrami macrokinetic model was carried out by directly fitting the experimental $\theta(t)$ data to Eq. (2) (shown in Fig. 1 as solid lines) using a non-linear multi-variable regression program [39]. Figs. 4 and 5, respectively illustrate plots of the Avrami exponent n_a and the Avrami crystallization rate constant K_a obtained as a result of the best fits as a function of the fusion temperature T_f for all of the s-PP resins studied. According to Fig. 4, the Avrami exponent n_a calculated for $\theta(t) \in [0.1, 0.8]$ was found to range from ca. 2.5 to 4.2 for s-PP#1, from ca. 2.2 to 2.9 for s-PP#2, and from ca. 1.9 to 3.2 for s-PP#4, respectively. Apparently, within the range $T_f \leq$ ca. 160°C the observed n_a values for all of the resins studied were found to scatter systematically with the fusion temperature used to melt the samples, while they were found to be independent of the fusion temperature within the range $T_f \geq$ ca. 160°C (despite slight scattering in the n_a data obtained for s-PP#1 resin).

Similar to the case of the reciprocal half-time $t_{0.5}^{-1}$ (see Fig. 3), values of the Avrami crystallization rate K_a, shown in Fig. 5, were also found to be strongly affected by changes in the fusion temperature used within the range $T_f \leq$ ca. 160°C, while they became independent of the fusion temperature used and assume a constant value within the range $T_f \geq$ ca. 160°C. The similarity between

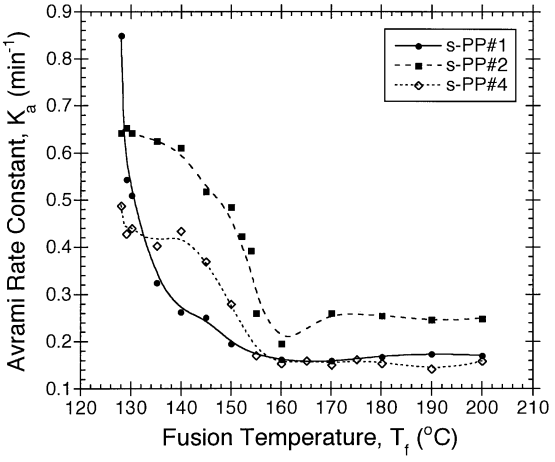

Fig. 5. Variation of the Avrami rate constant K_a as a function of the fusion temperature T_f used to melt the samples for all of the s-PP resins studied.

the reciprocal half-time $t_{0.5}^{-1}$ and the Avrami crystallization rate K_a is not surprising, since the Avrami crystallization rate K_a can be calculated directly from the reciprocal half-time $t_{0.5}^{-1}$ according to the following equation:

$$K_a = (\ln 2)^{1/n_a} t_{0.5}^{-1}. \quad (4)$$

The calculated values of the Avrami rate constant, though not shown, were found to be in good agreement with the experimental values, with the calculated values being $-1.3 \pm 3.7\%$ for s-PP#1, $2.0 \pm 0.9\%$ for s-PP#2 resin, and $1.8 \pm 4.2\%$ for s-PP#4 resin different from the experimental values on average.

4.2.2. Urbanovici–Segal analysis

Similar to the case of the Avrami analysis, data analysis based on the Urbanovici–Segal macrokinetic model was carried out by directly fitting the experimental $\theta(t)$ data to Eq. (3) (shown for example in Fig. 1 as dashed lines) using a non-linear multi-variable regression program [39]. Figs. 6–8, respectively, illustrate plots of the Urbanovici–Segal exponent n_{us}, the Urbanovici–Segal crystallization rate constant K_{us}, and the parameter r obtained as a result of the best fits as a function of the fusion temperature T_f for all of the s-PP resins studied. According to Fig. 6, the Urbanovici–Segal exponent n_{us} calculated for $\theta(t) \in [0.1, 0.8]$ was found to range from ca. 2.8 to 5.3 for s-PP#1, from ca. 2.5 to 4.7 for s-PP#2, and from ca. 2.0 to 4.8 for s-PP#4, respectively. Similar to the previous case, within the range $T_f \leq$ ca. 160°C the observed n_{us} values for all of the resins studied were found to scatter systematically with the fusion temperature used to melt the samples, while they were found to be independent of the fusion temperature within the range $T_f \geq$ ca. 160°C (despite slight scattering in the n_{us} data obtained for s-PP#1 and s-PP#2 resins).

Similar to the cases of the reciprocal half-time $t_{0.5}^{-1}$ (see Fig. 3) and the Avrami crystallization rate K_a, values of the

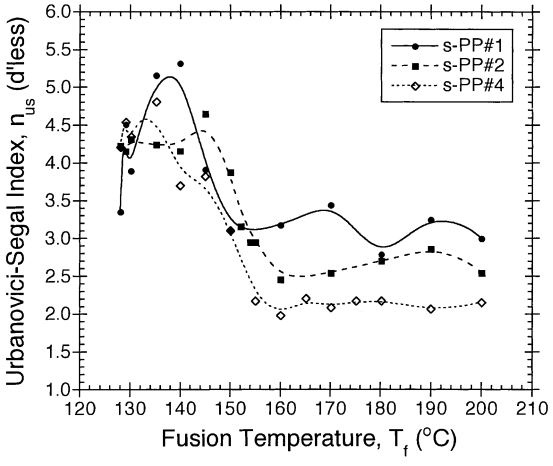

Fig. 6. Variation of the Urbanovici–Segal index n_{us} as a function of the fusion temperature T_f used to melt the samples for all of the s-PP resins studied.

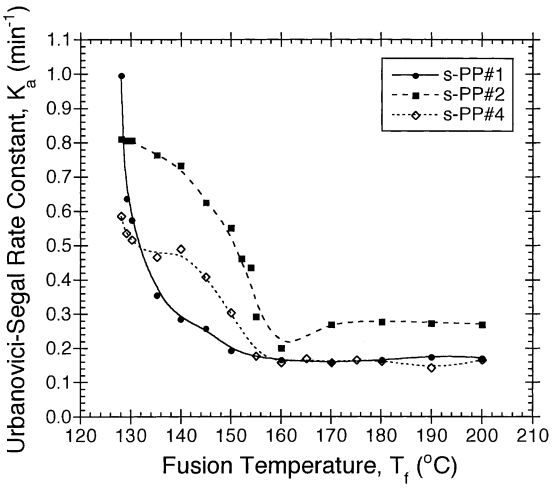

Fig. 7. Variation of the Urbanovici–Segal rate constant K_a as a function of the fusion temperature T_f used to melt the samples for all of the s-PP resins studied.

Urbanovici–Segal crystallization rate K_{us}, shown in Fig. 7, were also found to be strongly dependent on changes in the fusion temperature used within the range $T_f \leq$ ca. 160°C, while they became independent of the fusion temperature used and assume a constant value within the range $T_f \geq$ ca. 160°C. In fact, the similarity between the reciprocal half-time $t_{0.5}^{-1}$ and the Urbanovici–Segal crystallization rate K_{us} is not surprising, since the Urbanovici–Segal crystallization rate K_{us} can be calculated directly from the reciprocal half-time $t_{0.5}^{-1}$ according to the following equation:

$$K_{us} = \left(\frac{0.5^{(1-r)} - 1}{r - 1} \right)^{1/n_{us}} t_{0.5}^{-1}. \quad (5)$$

The calculated values of the Urbanovici–Segal rate constant, though not shown, were found to be in good agreement with the experimental values, with the calculated

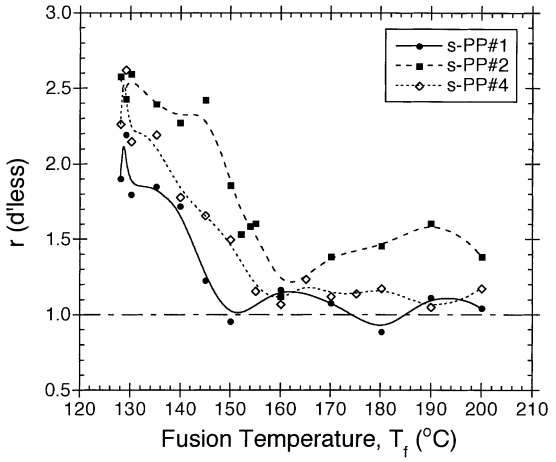

Fig. 8. Variation of the parameter r as a function of the fusion temperature T_f used to melt the samples for all of the s-PP resins studied.

values being $-2.0 \pm 3.3\%$ for s-PP#1, $0.3 \pm 0.9\%$ for s-PP#2 resin, and $0.8 \pm 4.2\%$ for s-PP#4 resin different from the experimental values on average.

Comparison between the kinetics parameters obtained from fitting experimental data to the Avrami and Urbanovici–Segal models (see Figs. 4–8) indicated that the extent of the discrepancies between the Urbanovici–Segal and Avrami kinetics parameters depends solely on the values of the parameter r obtained from the fits. It was stated earlier in this manuscript that the Urbanovici–Segal model becomes identical to the Avrami model when r approaches 1 [31]. By referring to Figs. 4–8, it is evident that, when $r > 1$, the values of the Urbanovici–Segal kinetics parameters are systematically greater than those of the Avrami ones, and as the greater the value of r is from 1, the greater the values of the Urbanovici–Segal kinetics parameters are than those of the Avrami ones. On the contrary, when $r < 1$, the values of the Urbanovici–Segal kinetics parameters are systematically less than those of the Avrami ones, and as the lesser the value of r is from 1, the lesser the values of the Urbanovici–Segal kinetics parameters are than those of the Avrami ones.

4.3. Effect of fusion temperature on lamellar morphology and melting behavior

The objectives of the WAXD experiment are two-fold: (1) it is to investigate whether or not the partial or complete melting conditions affect the formation of crystals during crystallization, and (2) it is to investigate whether or not the partial or complete melting conditions affect the amount of crystalline content formed. Fig. 9 illustrates WAXD diffractograms for the 'test' samples (i.e. the s-PP#2 samples isothermally crystallized in a Mettler hot-stage at $T_c = 85$°C after being partially melted at the fusion temperatures T_f of 130, 135, 140, 145, and 150°C or completely melted at T_f's of 160 and 180°C for a fixed holding time t_h of 5 min). It should be noted that the WAXD scan for the 'blank' sample was also shown in Fig. 9 for comparison and was labelled as 'blank.'

According to Fig. 9, all of the diffractograms exhibit major characteristic crystalline peaks at the scattering angles $2\theta = 12.32 \pm 0.09$, 16.01 ± 0.10, 20.70 ± 0.10, and 24.70 ± 0.08°, respectively. This clearly suggested that the crystalline structure of the 'test' and the 'blank' samples are essentially similar. According to related published work on crystallographical studies of s-PP [40–55], the crystalline structure of these samples deduced from the diffractograms shown in Fig. 9 can be best described by the limit-disordered form I [46,48,50] (after the most recent nomenclature by De Rosa et al. [55]), which is designated as an orthorhombic unit cell with axes $a = 14.5$, $b = 5.6$, and $c = 7.4$ Å and exhibits an antichiral packing of chains only along the a axis. The space group proposed for this crystal modification was *Pcaa* [41,47]. According to this space group, the major characteristic WAXD peaks should be

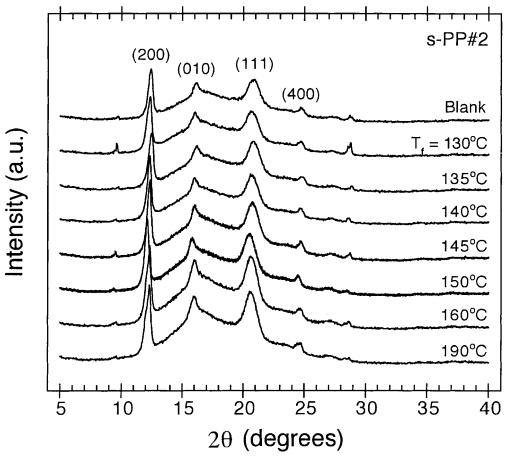

Fig. 9. WAXD patterns of s-PP#2 samples isothermally crystallized at 85°C after being melted at each respective fusion temperature T_f for 5 min. WAXD pattern of the as-prepared film is also shown for comparison and is labelled as 'blank.'

observed at the scattering angles $2\theta = 12.2$, 15.8, 20.8, and 24.5°, which correspond to the reflection planes at (200), (010), (111), and (400), respectively.

One simple method for estimating the apparent degree of crystallinity from a one-dimensional power WAXD pattern is to compute the integrated intensities of the pattern associated with the crystalline structures and the amorphous halo. To a first approximation, the degree of crystallinity is obtained by an assumption that the total scattering within a certain region of reciprocal space is independent of the state of aggregation of the materials [56]. The degree of crystallinity χ_c^{WAXD} is therefore expressed by the mass fraction of crystalline aggregates, and can be determined from the WAXD patterns based on the ratio of the integrated intensities under the crystalline peaks A_c to the integrated total intensities (i.e. $A_t = A_c + A_a$ where A_a is the integrated intensities under the amorphous halo): that is

$$\chi_c^{WAXD} = \frac{A_c}{(A_c + A_a)} \in [0, 1]. \tag{6}$$

Quantitatively, the results shown in Fig. 9 suggested that the WAXD degree of crystallinity χ_c^{WAXD} for all of the 'test' samples was found to be comparable (i.e. $\chi_c^{WAXD} = 0.32 \pm 0.01$), while that for the 'blank' sample was found to be a bit lower (i.e. $\chi_c^{WAXD} = 0.30$).

Fig. 10 shows the Lorentz-corrected SAXS intensity profiles (i.e. Kratky plots) of the experimental SAXS intensity profiles obtained on the same set of samples used in the WAXD measurement. With an assumption of a two-phase system comprising crystalline and amorphous fractions with sharp interfaces, the average value of the long period of the lamellar morphology (hereafter called the long period L_B) can be estimated from the maximum value of the scattering vector q_{max} observed in the Lorentz-corrected SAXS scattering profiles. According to

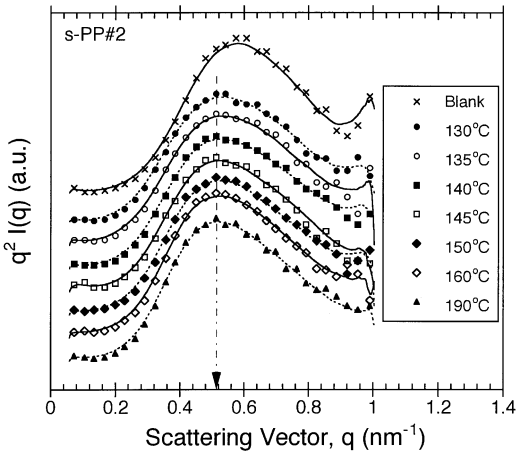

Fig. 10. Lorentz-corrected SAXS profiles (i.e. Kratky plots) of s-PP#2 samples isothermally crystallized at 85°C after being melted at each respective fusion temperature T_f for 5 min. Lorentz-corrected SAXS profile of the as-prepared film is also shown for comparison and is labelled as 'blank'.

Bragg's law and the mathematical definition of the scattering vector q, the long period L_B can then be calculated from the following equation:

$$L_B = \frac{2\pi}{q_{max}} \tag{7}$$

Quantitatively, the results shown in Fig. 10 suggested that the Lorentz-corrected SAXS scattering profiles for the 'test' samples were found to have a very comparable maximum value of the scattering vector q_{max} (i.e. $q_{max} = 0.519 \pm 0.006\ nm^{-1}$), while that for the 'blank' sample was found to have a maximum at $q_{max} = 0.581\ nm^{-1}$. These correspond to the values of the long period L_B of ca. 12.1 nm for all of the 'test' sample and 10.8 nm for the 'blank' sample.

Fig. 11 illustrates DSC heating scans (20°C min^{-1}) obtained on the same set of samples used in both the WAXD and SAXS measurements. Evidently, there are two major melting endotherms present on all of the heating scans. According to a recent work [57], the two melting endotherms were designated as (1) low-temperature melting endotherm (the peak temperature of which was denoted in Ref. [57] as the low-melting peak temperature T_{ml}) which corresponds to the melting of the primary crystallites formed at the crystallization temperature T_c, and (2) the high-temperature melting endotherm (the peak temperature of which is denoted in Ref. [57] as the high-melting peak temperature T_{mh}) which corresponds to the melting of the crystallites re-crystallized during a heating scan. Quantitatively, the results shown in Fig. 11 suggested that the positions of the low and the high-temperature melting endotherms for the 'test' samples crystallized at T_c = 85°C after being partially or completely melting at T_f ranging from 130 to 190°C were found to be superimposable on one another, with the average values of T_{ml} and T_{mh} being 117.0 ± 0.3 and 125.9 ± 0.2°C, respectively. However, the positions of the two endotherms for the 'blank' sample were found to shift toward lower temperature, with the values of T_{ml} and T_{mh} being 114.2 and 124.7°C, respectively. This finding suggested that the crystallites formed in the 'blank' samples were less stable than those formed in the 'test' samples.

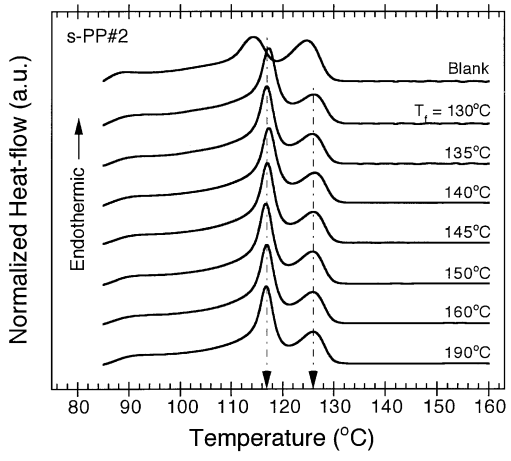

Fig. 11. Subsequent melting thermograms (20°C min^{-1}) of s-PP#2 samples isothermally crystallized at 85°C after being melted at each respective fusion temperature T_f for 5 min. Subsequent melting thermogram of the as-prepared film is also shown for comparison and is labelled as 'blank'.

If the assumption of the two-phase system is valid for describing the lamellar morphology of s-PP samples isothermally crystallized according to the conditions prescribed in this manuscript, the thickness of mature crystals l_c (hereafter called the lamellar thickness) can be estimated as the multiplication product of the WAXD degree of crystallinity χ_c^{WAXD} and the long period L_B: that is

$$l_c = L_B \chi_c^{WAXD} \tag{8}$$

According to the WAXD and SAXS results, the lamellar thickness l_c for all of the 'test' samples were estimated to be ca. 3.9 nm, while that for the 'blank' sample was ca. 3.2 nm. This finding clearly confirmed the hypothesis drawn at the end of the previous paragraph that the crystallites formed in the 'blank' samples were less stable than those formed in the 'test' samples.

5. Conclusions

In this manuscript, the effect of fusion temperature on isothermal crystallization, comprising the kinetics and the lamellar morphological aspects of the process, and subsequent melting behavior of three commercial grade s-PP resins was thoroughly investigated using a combination of DSC, WAXD, and SAXS techniques. On partial melting, the DSC experiment suggested that the choice of the fusion temperatures used to melt the samples plays an important role in determining the overall rate of isothermal

crystallization, in which all the crystallization rate parameters studied ($t_{0.5}^{-1}$, K_a, and K_{us}) were found to decrease monotonically with an increase in the value of the fusion temperature T_f used. The decrease in the values of these rate parameters with T_f continues up to a critical value (i.e. $T_f^{cr} \approx 160$°C), at which point the values of all the rate parameters approach a constant value (i.e. approaching the complete melting condition). Interestingly, despite the much difference in the molecular weight characteristics among these resins, the critical values of the fusion temperature T_f required for assuring the complete melting conditions (for a fixed holding time t_h of 5 min at T_f) of these resins are technically identical (i.e. ca. 160°C).

In addition to the DSC experiment, the WAXD/SAXS/DSC experiment showed that values of the apparent crystallinity content χ_c^{WAXD}, the long period L_B, the lamellar thickness l_c, and the low-melting peak temperature T_{ml} of the 'blank' sample were respectively less than those of the 'test' sample, suggesting that the crystallites formed in the 'blank' sample were less stable than those formed in the 'test' samples, and that the choice of the fusion temperatures used to melt the samples has no effect on the resulting values of the apparent crystallinity content χ_c^{WAXD}, the long period L_B, the lamellar thickness l_c, and the low-melting peak temperature T_{ml}. This finding is in fact very important, since it suggested to us that even though the crystallites formed in the 'blank' sample were less stable than those formed in the 'test' samples, on partial melting, these less stable (i.e. thinner lamella) crystalline residues can readily enhance the overall crystallization rate (viz. the degree of the enhancement is dictated by the concentration of the crystalline residues which is, in turn, determined by the choice of the fusion temperature T_f used) by acting as predetermined athermal nucleation sites which result in the formation of the more stable (i.e. thicker lamella) crystallites during subsequent crystallization at $T_c = 85$°C.

Acknowledgements

We would like to thank Dr Joseph Schardl of Fina Oil and Chemical Company (Dallas, Texas, USA) for supplying the s-PP resins used in this study, and Dr Roger A. Phillips and his co-workers of Basell USA, Inc. (Elkton, Maryland, USA) for performing molecular characterizations of the resin. The research at Oak Ridge was sponsored in part by the US Department of Energy under contract number DE-AC05-00OR22725 with the Oak Ridge National Laboratory (ORNL), managed by the UT Battelle, LLC. In addition, PS would like to acknowledge a grant provided by Chulalongkorn University through the Development Grants for New Faculty/Researchers. Lastly, parts of the experimental work carried out at the Department of Materials Science and Engineering, the University of Tennessee are greatly acknowledged.

References

[1] Wunderlich B. Macromolecular physics, vol. 2. New York: Academic Press, 1976. p. 52–70.
[2] Turska E, Gogolewski S. J Appl Polym Sci 1975;19:637.
[3] Khanna YP, Reimschuessel AC. J Appl Polym Sci 1988;35:2259.
[4] Khanna YP, Reimschuessel AC, Banerjie A, Altman C. Polym Engng Sci 1988;28:1600.
[5] Khanna YP, Kumar R, Reimschuessel AC. Polym Engng Sci 1988;28:1607.
[6] Khanna YP, Kumar R, Reimschuessel AC. Polym Engng Sci 1988;28:1612.
[7] Khanna YP, Kuhn WP, Macur JE, Messa AF, Murthy NS, Reimschuessel AC, Schneider RL, Sibilia JP, Signorelli AJ, Taylor TJ. J Polym Sci, Polym Phys 1995;33:1023.
[8] Mehl NA, Rebenfeld L. Polym Engng Sci 1992;32:1451.
[9] Fillon B, Wittmann JC, Lotz B, Thierry A. J Polym Sci, Polym Phys 1993;31:1383.
[10] Fillon B, Lotz B, Thierry A, Wittmann JC. J Polym Sci, Polym Phys 1993;31:1395.
[11] Fillon B, Thierry A, Wittmann JC, Lotz B. J Polym Sci, Polym Phys 1993;31:1407.
[12] Ziabicki A, Alfonso GC. Colloid Polym Sci 1994;272:1027.
[13] Alfonso GC, Ziabicki A. Colloid Polym Sci 1995;273:317.
[14] Alfonso GC, Scardigli P. Macromol Symp 1997;118:323.
[15] Feng Y, Jin X. J Appl Polym Sci 1999;72:1559.
[16] Supaphol P, Spruiell JE. J Appl Polym Sci 2000;75:337.
[17] Hay JN, Sabir M. Polymer 1969;10:203.
[18] Hay JN, Fitzgerald PA, Wiles M. Polymer 1976;17:1015.
[19] Hay JN. Brit Polym J 1979;11:137.
[20] Kolmogorov AN. Izv Akad Nauk USSR, Ser Math 1937;1:355.
[21] Johnson WA, Mehl KF. Trans Am Inst Min Met Engng 1939;135:416.
[22] Avrami M. J Chem Phys 1939;7:1103.
[23] Avrami M. J Chem Phys 1940;8:212.
[24] Avrami M. J Chem Phys 1941;9:177.
[25] Evans UR. Trans Faraday Soc 1945;41:365.
[26] Ding Z, Spruiell JE. J Polym Sci, Polym Phys 1997;35:1077.
[27] Tobin MC. J Polym Sci, Polym Phys 1974;12:399.
[28] Tobin MC. J Polym Sci, Polym Phys 1976;14:2253.
[29] Tobin MC. J Polym Sci, Polym Phys 1977;15:2269.
[30] Malkin AY, Beghishev VP, Keapin IA, Bolgov SA. Polym Engng Sci 1984;24:1396.
[31] Urbanovici E, Segal E. Thermochim Acta 1990;171:87.
[32] Supaphol P. Thermochim Acta 2001;370:37.
[33] Wunderlich B. Macromolecular physics, vol. 2. New York: Academic Press, 1976. p. 132–147.
[34] Wignall GD, Lin J-S, Spooner S. J Appl Cryst 1990;23:241.
[35] Hendricks RW. J Appl Cryst 1978;11:15.
[36] Russell TP, Lin J-S, Spooner S, Wignall GD. J Appl Cryst 1988;21:629.
[37] Supaphol P, Spruiell JE. J Appl Polym Sci 2000;75:44.
[38] Supaphol P. J Appl Polym Sci 2000;78:338.
[39] Supaphol P, Spruiell JE. J Macromol Sci-Phys 2000;B39:257.
[40] Corradini P, Natta G, Ganis P, Temussi PA. J Polym Sci 1967;C16:2477.
[41] Lotz B, Lovinger AJ, Cais RE. Macromolecules 1988;21:2375.
[42] Lovinger AJ, Lotz B, Davis DD. Polymer 1990;31:2253.
[43] Chatani Y, Maruyama H, Noguchi K, Asanuma T, Shiomura T. J Polym Sci 1990;C28:393.
[44] Lovinger AJ, Davis DD, Lotz B. Macromolecules 1991;24:552.
[45] Chatani Y, Maruyama H, Asanuma T, Shiomura T. J Polym Sci, Polym Phys 1991;29:1649.
[46] Lovinger AJ, Lotz B, Davis DD, Padden FJ. Macromolecules 1993;26:3494.
[47] De Rosa C, Corradini P. Macromolecules 1993;26:5711.

[48] Auriemma F, De Rosa C, Corradini P. Macromolecules 1993;26:5719.
[49] De Rosa C, Auriemma F, Corradini P. Macromolecules 1996;29:7452.
[50] De Rosa C, Auriemma F, Vinti V. Macromolecules 1997;30:4137.
[51] Lovinger AJ, Lotz B. J Polym Sci, Polym Phys 1997;35:2523.
[52] Auriemma F, De Rosa C, Ruiz de Ballesteros O, Vinti V, Corradini P. J Polym Sci, Polym Phys 1998;36:395.
[53] De Rosa C, Auriemma F, Vinti V, Grassi A, Galimberti M. Polymer 1998;39:6219.
[54] De Rosa C, Auriemma F, Vinti V. Macromolecules 1998;31:7430.
[55] De Rosa C, Talarico G, Caporaso L, Auriemma F, Galimberti M, Fusco O. Macromolecules 1998;31:9109.
[56] Ryan AJ, Stanford JL, Bras W. Nye TMW Polymer 1997;38:759.
[57] Supaphol P. J Appl Polym Sci 2001. In press.